01 Jan 2023

# Multi-Point Optical Fiber Fabry-Perot Curvature Sensor Based On Microwave Photonics

Chen Zhu
*Missouri University of Science and Technology*, cznwq@mst.edu

Ruimin Jie

Osamah Alsalman

Hongkun Zheng

*et. al. For a complete list of authors, see https://scholarsmine.mst.edu/ele_comeng_facwork/5047*



## Recommended Citation

C. Zhu et al., "Multi-Point Optical Fiber Fabry-Perot Curvature Sensor Based On Microwave Photonics," *Journal of Lightwave Technology*, Institute of Electrical and Electronics Engineers; Optica, Jan 2023.
The definitive version is available at https://doi.org/10.1109/JLT.2023.3278742

# Multi-Point Optical Fiber Fabry-Perot Curvature Sensor Based on Microwave Photonics

Chen Zhu, *Member, IEEE,* Ruimin Jie, Osamah Alsalman, Hongkun Zheng, Wassana Naku, Bo Liu, and Lingmei Ma

***Abstract*—This article reports a multi-point curvature sensor system based on multiplexed optical fiber Fabry-Perot interferometric (FPI) sensor devices and a microwave photonics interrogation technique. The FPI sensor is fabricated with the assistance of a capillary tube, where a short section of the capillary is sandwiched between two single-mode fibers, forming the air-gap Fabry-Perot cavity. Bending of the FPI device leads to changes in the fringe contrast of its reflection spectrum. Based on the microwave photonics filtering technique, variations of the fringe contrast are encoded into the changes in the peak magnitude of the passband in the frequency response of the FPI device. By multiplexing such FPI devices with different cavity lengths, multi-point measurements of curvature can be realized by tracking changes in corresponding passbands in the frequency response of the system. The FPI curvature sensor is easy-to-manufacture and cost-effective, and the microwave photonics-based system provides an alternative and robust solution to interrogating the multiplexed FPI sensors for multi-point curvature sensing that could be desired in structural health monitoring, human-machine interface sensing, and other related fields.**

***Index Terms*—Microwave photonics; Fabry-Perot interferometer; curvature sensor; multiplexing.**

## I. Introduction

Accurate measurements of deformation/curvature are of significant importance in a variety of fields [1]. For example, in structural health monitoring, the curvature provides critical information regarding the health status of the structure under investigation [2, 3]; in the field of medical application, real-time monitoring of the bending of a needle during surgery or *in-vivo* treatment is desired because it indicates whether the needle tip has reached upon the target tissue or not [4, 5]; in human-machine interface perception, sensing of local deformation (a localized bending) reveals the existence of an external perturbation [6, 7]. Curvature sensors that are based on fiber optics, being light in weight, small in size, embeddable, and immune to electromagnetic interference, have attracted wide interest in recent years [8, 9].

The majority of the reported optical fiber curvature sensors in literature are point-wise sensors, i.e., only capable of single-point measurements [8]. These sensors are mainly based on optical fiber modal interferometers. Bending of the interferometer results in changes in the refractive index distribution of the optical fiber section along the radial direction and ultimately leads to shifts in the interferogram. The measurement of curvature can thus be realized by monitoring the spectral shift of the modal-interferometer-based device. There are a few limiting aspects of these devices. For instance, the construction of such a modal interferometer is relatively complicated, requiring the integration of several different types of optical fibers, such as single-mode fibers [10, 11], multimode fibers [12-14], multi-core fibers [15-17], etc. In addition, the length of the device is typically at least a few cm. Moreover, multiplexing of multiple such modal interferometers is quite challenging, thus making multi-point sensing of curvature difficult. Fiber Bragg gratings (FBGs) have also been configured as curvature sensors [18-22]. On one hand, the curvature is encoded into the reflected power from the FBG. For this type of device, a mode exciter, e.g., a section of multimode fiber, is required to excite cladding modes [23, 24]. On the other hand, an FBG can be embedded into a soft matrix, where bending/deformation of the soft material changes the strains applied to the FBG, leading to Bragg wavelength shifts in its reflection spectrum [18, 19, 25]. Multiplexing of this type of FBG curvature sensor can be easily achieved using FBGs with different Bragg wavelengths based on wavelength-division multiplexing. However, the measurement sensitivity of FBG-based curvature sensors is relatively low compared to interferometric sensors. Also, the length of an FBG is relatively large on the order of a mm scale.

The optical fiber Fabry-Perot interferometer (FPI) is a great candidate for the development of miniature sensor devices, as a fiber-inline Fabry-Perot cavity is only a few hundred μm in length or less. Although optical fiber FPI-based curvature sensors were reported previously, FPI-based multi-point sensing has not been demonstrated yet. Indeed, several FPIs with different cavity lengths can be multiplexed in a system, and a simple and widely-used approach, i.e., frequency-division multiplexing (FDM), can be employed for the demodulation of the superimposed signal to achieve multi-point sensing. However, the FDM-based demodulation approach requires a delicate interrogation system (e.g., an ultra-broadband light source and a bulky spectrum analyzer) and complicated signal processing. Very recently, a new

This work was supported in part by Center-initiated Research Project of Zhejiang Lab (No. K2022ME0AL05) and Research Initiation Project of Zhejiang Lab (No. 2022ME0PI01).

Chen Zhu, Ruimin Jie, Hongkun Zheng, Bo Liu and Lingmei Ma are with the Research Center for Optical Fiber Sensing, Zhejiang Lab, Hangzhou 311100, China. (Corresponding author: Chen Zhu, chenzhu@zhejianglab.com)

Osamah Alsalman is with the Department of Electrical Engineering, College of Engineering, King Saud University, P.O.Box 800, Riyadh 11421, Saudi Arabia.

Wassana Naku is with the Department of Electrical and Computer Engineering, Missouri University of Science and Technology, Rolla, MO 65409, USA.

technique based on microwave photonics filtering (MPF) was demonstrated for interrogating multiplexed Fabry-Perot strain sensors [26]. Multiple FPIs were identified based on the discrete passbands in the radiofrequency (RF) response of the system. Changes in the tensile strains exerted on the FPI sensor resulted in changes in its cavity length, leading to variations in the central frequency of the corresponding RF passband. However, the MPF-based demodulation sensitivity is quite low, orders of magnitude lower than the spectral shift-based method in the optical domain.

In this article, we propose and experimentally demonstrate a multi-point optical fiber curvature sensor system based on microwave photonics. The individual curvature sensor is miniature, based on an air-cavity FPI, where a short capillary tube is spliced between two single-mode fibers (SMFs). Bending of the FPI sensor causes decreases in the fringe visibility of the reflection spectrum. The changes in the fringe visibility are then measured based on the MPF technique, where the magnitude of the passband decreases with decreasing fringe visibility. It is shown that the sensitivity of the MPF-based demodulation is comparable to the optical-domain-based method. By multiplexing a few such FPIs with different cavity lengths in parallel, multi-point sensing of curvature can be realized by identifying variations in the magnitude of the discrete passbands in the RF response.

The rest of the paper is organized as follows. In section II, the working principle of the FPI sensor for curvature sensing and the MPF technique for demodulation are shown in detail. Simulations are performed to verify the proposed technique. In section III, proof-of-concept experiments for measuring variations of curvature based on the proposed sensor system are performed. Section IV concludes this paper.

## II. Principle

A schematic diagram of the proposed sensor system is given in Fig. 1, including the FPI-based multi-point curvature sensor and the MPF-based interrogator. An optical spectrum analyzer (OSA) is also included in the system for performance comparison, as it will be shown later. A low-coherent light source is employed for generating the probing light, which is routed into the multiplexed sensor via a circulator and an optical splitter. The reflected light from the multiplexed sensors is then directed into an optical coupler via the circulator. A small portion of the light signal (e.g., 10%) is received by the OSA. The rest (i.e., 90%) arrives at an electro-optic modulator (EOM), where the signal is amplitude-modulated by a microwave signal coming from Port 1 of a vector network analyzer (VNA). The modulated light first gets boosted at an erbium-doped fiber amplifier (EDFA) and then goes through a long length of dispersion-compensating fiber (DCF) or simply a long length of SMF, and is finally received by a highspeed photodetector (PD). The obtained electrical signal from the PD is sent into Port 2 of the VNA. As such, synchronized detection at the modulation microwave frequency can be achieved. The complex frequency response of the multiplexed curvature sensor can then be obtained by sweeping the modulation microwave frequency and recording the S21 parameter from the VNA.

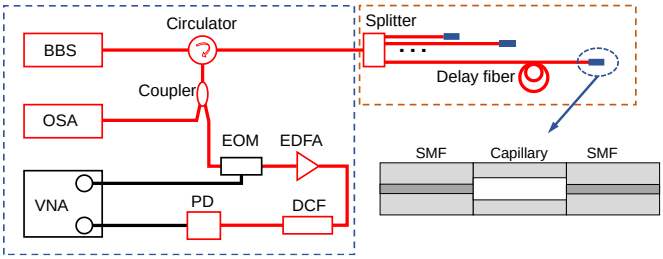


Fig. 1. Schematic diagram of the proposed microwave photonics-based multi-point curvature sensor system. The blue rectangular box represents the interrogator, and the orange box indicates the multi-point sensor. A detailed view of the sensor is also given. BBS, optical broadband source; OSA, optical spectrum analyzer; VNA, vector network analyzer; EOM, electro-optic modulator; EDFA, erbium-doped fiber amplifier; PD, photodetector; DCF, dispersion compensating fiber; SMF, single-mode fiber.

The reflection from the multiplexed FPI sensors can be expressed as

$$R(\omega)=\sum_{i=1}^{N}\left[1+V_i\cos\left(\frac{\omega}{c}\cdot 2nL_i\right)\right] \tag{1}$$

where $N$ denotes the number of sensors included in the system; $\omega$ is the angular frequency of the optical signal; $c$ is the speed of light in vacuum; $n$ is the refractive index of the cavity medium (air); $L_i$ denotes the length of the $i$-th FPI sensor; and, $V_i$ is the visibility of the interference of the $i$-th FPI sensor. Note that Eq. (1) is obtained on the basis of optical coherent operation for each of the sensors, while the superposition of the reflected signals from any two sensors is operated under an incoherent regime to avoid interference between sensors. This can be achieved by using lead-in delay fibers shown in Fig. 1 with lengths that are sufficiently larger than the coherence length of the light source.

The reflected optical signal from the FPI sensors given in Eq. (1) is then sent into the EOM for intensity modulation, followed by amplification, delay control, and optoelectronic conversion. The overall frequency response for double-side-band modulation is given by

$$H(\Omega)=\int R(\omega)\left[mH^*(\omega)\cdot H(\omega+\Omega)+mH(\omega)\cdot H^*(\omega-\Omega)\right]d\omega \tag{2}$$

where $\Omega$ denotes the angular frequency of the microwave modulation signal; $m$ is the modulation index; and, $H(\omega)$ represents the transfer function of the delay line in the system. Given the fact that a broadband optical signal is of interest in the system, a broadband delay line (e.g., a length of fiber) is used. Thus, the overall frequency response given in Eq. (2) can be considered the superposition of several RF single passband filters [27]. The central frequency of each passband is uniquely determined by the cavity length of the corresponding FPI sensor and can be expressed as

$$f_i=\frac{1}{D_{DCF}FSR} \tag{3}$$

where $D_{DCF}$ denotes the dispersion coefficient of the DCF used in the system with the unit of ps/nm and $FSR$ represents the free spectral range of the interferogram of the FPI. Thus, the

reflection spectrum of each FPI sensor is encoded into the characteristics (e.g., peak frequency, amplitude, etc.) of the corresponding RF passband in the frequency response.

When the FPI sensor shown in Fig. 1 is bent, the fringe visibility ($V$) of its reflection spectrum will decrease significantly due to the leakage of the light in the capillary. The decrease in the fringe visibility will consequently lead to a decrease in the amplitude of the corresponding RF passband in the frequency response, according to Eq. (2). Thus, curvature sensing using the FPI sensor is made possible based on its frequency response. Numerical simulations are performed to verify the proposed concept. Fig. 2(a) gives the calculated reflection spectra of an FPI sensor with different values of fringe visibility based on Eq. (1). Fig. 2(b) shows the corresponding RF responses of the FPI sensor. Single passbands are revealed. Importantly, the magnitude at the center frequency of the passband decreases as the fringe visibility decreases, as expected.

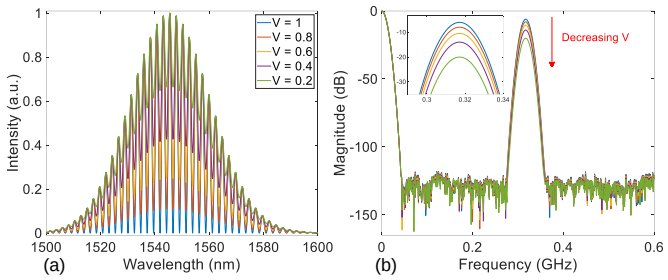


Fig. 2. Simulation results demonstrating the proposed concept for single-point sensing. (a) Reflection spectra of an FPI sensor with different fringe visibility. (b) Frequency responses. In the calculation, the cavity length of the FPI was set to 500 μm; the dispersion coefficient was -1320.1 ps/nm@1545 nm.

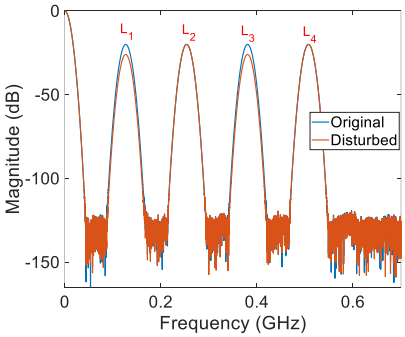


Fig. 3. Simulation results demonstrating the multi-point sensing capability of the proposed system.

By multiplexing several such FPI sensors with different cavity lengths in parallel and monitoring the multiple RF passbands simultaneously, multipoint curvature sensing can be realized. Fig. 3 plots the calculated frequency response of the system when four FPI sensors with different cavity lengths (i.e., $L_1$ = 200 μm, $L_2$ = 400 μm, $L_3$ = 600 μm, and $L_4$ = 800 μm) are multiplexed in parallel. The fringe visibility of the four FPI sensors is set to 0.8, representing an initial undisturbed case. Four discrete passbands are obtained in the frequency response, corresponding to the four different cavity lengths, denoted as $L_1$, $L_2$, $L_3$, and $L_4$; the larger the cavity length, the higher the center frequency of the RF passband, as can be expected from Eq. (3). Next, the fringe visibility of the two FPI sensors (i.e., $L_1$ and $L_3$) is decreased to simulate the case of an external perturbation (e.g., curvature variation), and the calculated frequency response is also included in Fig. 3. Decreases in the peak magnitude for $L_1$ and $L_3$ are observed, while the peak magnitude for $L_2$ and $L_4$ does not show any change, demonstrating the capability of the system for simultaneous multi-point sensing.

## III. Experimental Results and Discussion

### *A. Demonstration of curvature sensing based on a single interferometer*

A prototype FPI sensor device with a cavity length of ~780 μm was fabricated. The construction of the sensor is quite simple, involving three steps. First, a silica capillary was spliced to an SMF using a commercial fusion splicer based on a specially designed program to ensure good mechanical strength at the connection point and avoid significant collapse of the hollow tube. Secondly, the free end of the connected capillary was secured to a high-precision cleaving platform (mainly including an imaging system and an optical fiber cleaver), and was then cut off at a desired point. Finally, another SMF was connected to the cleaved end of the capillary to form the FPI sensor device. The high-precision cleaving platform made it possible to precisely control the length of the air cavity of the fabricated FPI with an accuracy of ~10 μm. The key components that were employed in the demodulation system are listed as follows: C-band broadband light source (1528~1563 nm); EOM, iXblue MXAN-LN-10; VNA, R&S®ZNB8; PD, KG-PD-20G; OSA, Yokogawa AQ6370D, dispersion module with a dispersion coefficient of -1320.1 ps/nm @1545 nm.

The measured frequency response of the single FPI sensor system is plotted in Fig. 4(a). The measured interferogram of the sensor from OSA is given in Fig. 4(b). The FSR of the interferogram shown in Fig. 4(b) is determined to be 1.545 nm, from which the cavity length is calculated to be 773 μm, as designed. Modulation envelopes can also be observed in the reflection spectrum, which is due to the anti-resonant guidance that occurred in the hollow capillary [28]. The envelope could distort the shape of the passband in the frequency response, but it will not affect the sensing performance significantly. Based on Eq. (3), the central frequency of the passband in the frequency response can be estimated to be 490 MHz, which is slightly different from the value of 465 MHz shown in Fig. 4(a). The approximately 5% discrepancy is attributed to the calculation errors of the FSR and the fluctuations of the dispersion coefficient at different wavelengths. The observable distortions of the passband in the frequency response are attributed to the high-order dispersion in the SMF and the uneven gain profile of the EDFA [26].

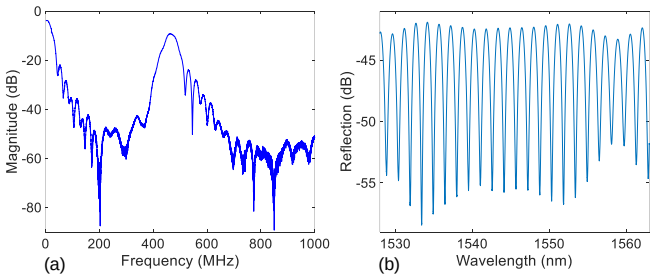

Fig. 4. Characterization of a prototype FPI sensor with a cavity length of ~770 µm. (a) Frequency response measured from the VNA. (b) Reflection spectrum measured from the OSA.

A curvature test was then carried out. The device was fixed to two translation stages (OMTOOLS, HFA-XYZ), and curvature was applied by moving one of the stages inwards to bend the FPI sensor. The initial distance between the two fixture points was 50 mm, and displacement in steps of 50 µm was applied. The measured frequency responses for different settings of curvature are given in Fig. 5(a). The amplitude of the frequency passband decreased as the applied curvature increased, which matched well with our expectation and the simulation results shown in Fig. 2.

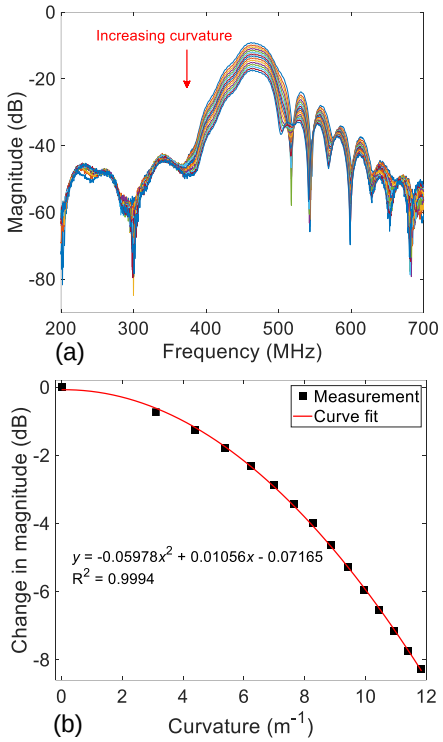


Fig. 5. Frequency responses of the single FPI device to variations of curvature. (a) Measured frequency responses for different settings of curvature. (b) The change in the peak amplitude of the passband as a function of curvature. A second-degree polynomial curve fit model was applied.

Fig. 5(b) plots the determined peak magnitude of the frequency passband as a function of the curvature in the calibrated range. A second-degree polynomial curve fit was applied to predict the relationship, and an R-squared of 0.9994 was revealed. The peak amplitude of the frequency response changed by ~8 dB in a curvature range of 0~12 $m^{-1}$. The optical responses of the sensor measured from OSA were also investigated, showing a total decrease of 10 dB in the fringe contrast as the applied curvature increased to 12 $m^{-1}$. Thus, the measurement sensitivity of the microwave photonics-based interrogation for the proposed curvature sensor is not significantly compromised in comparison to the conventional OSA-based approach. Note that in previous work [26, 29], sensing was achieved by tracking the shift of the peak frequency of the passband. However, the sensitivity of the peak frequency-based method was significantly sacrificed, orders of magnitude lower than the OSA-based analysis. The proposed system introduced a new direction in exploring the MPF technique for sensing applications by monitoring the peak amplitude variations in response to external perturbations. The stability of the FPI curvature sensor was demonstrated. Fig. 6 shows the measured changes in the peak amplitude of the frequency response in a time period of 5 mins, where a variation of only 0.01 dB was observed in the test, indicating good stability of the system. To further enhance the stability, a reference device (e.g., an FPI device arranged in parallel as shown in the next section) can be introduced to compensate for system and environmental noises.

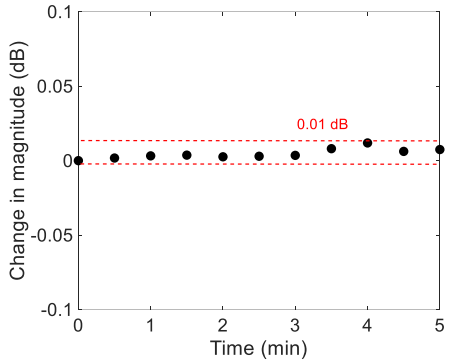


Fig. 6. Stability test of the single FPI sensor.

### *B. Demonstration of curvature sensing based on multiplexed interferometers*

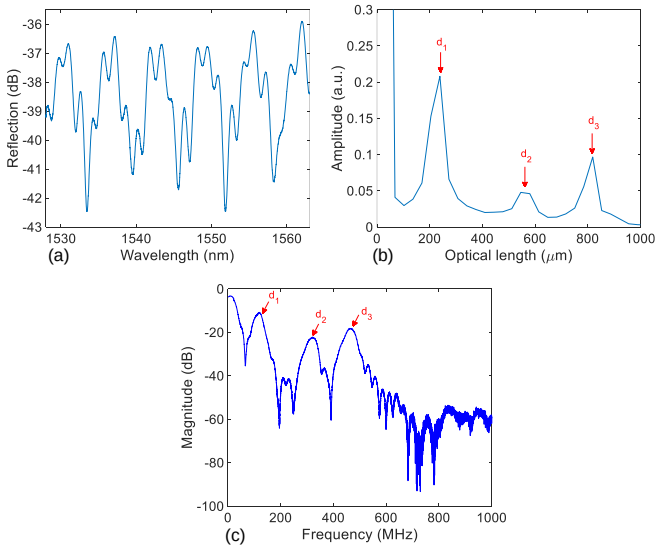


Fig. 7. Characterization of a multiplexed sensor system with three FPI sensors. (a) Reflection spectrum measured from the OSA. (b) Spatial domain signal obtained by applying a fast Fourier transform to the optical reflection spectrum. (c) Frequency response measured from the VNA.

Next, three such FPI sensors with different cavity lengths were multiplexed using an optical splitter and characterized by the system shown in Fig. 1. The measured optical reflection spectrum of the multiplexed sensor system is shown in Fig. 7(a). A relatively complicated interference pattern is obtained due to the superposition of the reflection signals from the three FPI devices. By applying the fast Fourier transform calculation to

the spectrum shown in Fig. 7(a), the spatial domain signal of the multiplexed sensor system can be obtained, as given in Fig. 7(b). Three distinct peaks are revealed in the spatial domain signal, corresponding to the three FPIs with different cavity lengths of ~200 μm, 540 μm, and 770 μm. The measured frequency response of the multiplexed sensor system from the VNA is plotted in Fig. 7(c), where three passbands can be observed. The central frequencies of the three passbands match well with the three different cavity lengths revealed in Fig. 7(b) according to Eq. (3).

Curvature was then applied to the third FPI (i.e., the cavity length is denoted as $d_3$). The measured frequency responses of the system to different curvatures are shown in Fig. 8(a). As can be seen, the peak amplitude of the passband corresponding to $d_3$ decreased with increasing curvature. The peak magnitude for the other two passbands did not show a significant dependence on the curvature variations applied to $d_3$, indicating little crosstalk between sensors. The specific relationship between the change in the peak magnitude and the curvature is shown in Fig. 8(b) and is quantified using a second-degree polynomial curve fit. The fitting results are indicated in the figure. The determined responses from the other two FPIs are also shown for comparison. Less than 3% crosstalk between sensors was observed in the calibrated curvature range.

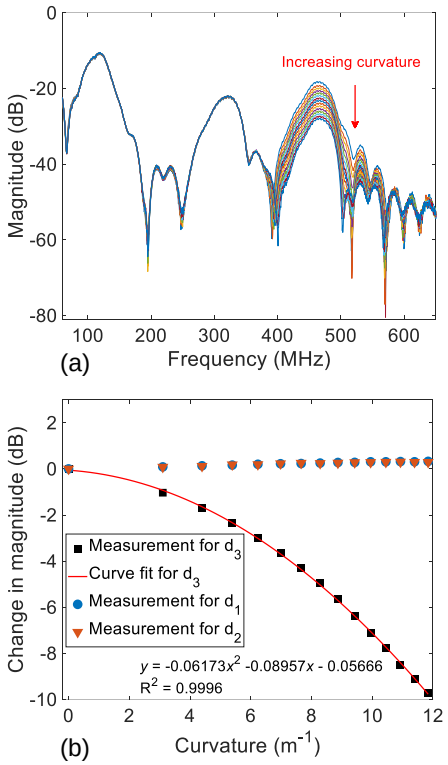


Fig. 8. Curvature sensing using the FPI with a cavity length of $d_3$. (a) Measured frequency responses for different settings of curvature. (b) The change in the corresponding peak magnitude as a function of curvature. A curve fit was applied. The responses from the other two FPIs are also shown for the purpose of comparison.

An additional experiment was performed to demonstrate the simultaneous multi-point sensing capability of the proposed sensor system. Four FPI sensors with different cavity lengths of approximately 309 μm, 573 μm, 770 μm, and 1042 μm (corresponding to S1, S2, S3, and S4) were multiplexed in parallel. The measured frequency response from the VNA is plotted in Fig. 9. Then, curvature was simultaneously applied to S1 and S3, while S2 and S4 were not disturbed. The corresponding response was recorded and is shown in Fig. 9. Changes in the two passbands corresponding to S1 and S3 can be observed, where no significant variations in the passbands corresponding to S2 and S4 are shown, as expected. The multiplexing capability of the system is related to the wavelength range of the optical source, the frequency measurement range of the VNA, and the dispersion coefficient of the dispersion module, and a detailed analysis can be found in [26].

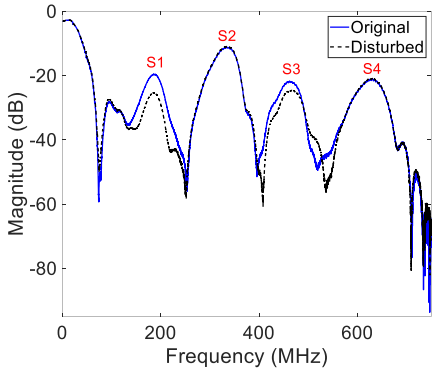


Fig. 9. Demonstration of the multi-point sensing capability of the proposed system. The blue solid curve represents the measured frequency response of the multiplexed sensor system without curvature applied, and the black dashed curve represents the frequency response when curvature was applied to two of the sensors (i.e., S1 and S3).

## IV. CONCLUSION

To conclude, we have proposed and experimentally demonstrated a multi-point curvature sensor system based on multiplexed optical fiber air-cavity FPI sensors. The MPF-based technique is employed to interrogate the multiplexed FPI sensors by measuring variations in the frequency response of the sensor system. In the proof-of-concept experiments, a single FPI device is first demonstrated for single-point measurements of curvature based on the MPF interrogation with comparable sensitivity to the OSA-based method. Multiple such FPI devices with different cavity lengths are then investigated for simultaneously multi-point curvature sensing with little crosstalk between sensors. The proposed sensor system provides an easy and robust approach for multipoint curvature measurements, which might find applications in structural health monitoring, mechanical engineering, and biomedical engineering.

## ACKNOWLEDGMENT

Researchers Supporting Project number (RSPD2023R654), King Saud University, Riyadh, Saudi Arabia.

## REFERENCES

[1] T. Li, D. Wu, M. O. Khyam, J. Guo, Y. Tan, and Z. Zhou, "Recent Advances and Tendencies regarding Fiber Optic Sensors for Deformation Measurement: A Review," *IEEE Sensors Journal*, 2021.

[2] J. Ma and A. Asundi, "Structural health monitoring using a fiber optic polarimetric sensor and a fiber optic curvature sensor-static

and dynamic test," *Smart materials and structures*, vol. 10, no. 2, p. 181, 2001.

[3] M. Z. Marković, J. S. Bajić, M. Vrtunski, T. Ninkov, D. D. Vasić, and M. B. Živanov, "Application of fiber-optic curvature sensor in deformation measurement process," *Measurement*, vol. 92, pp. 50-57, 2016.

[4] S. C. Ryu, Z. F. Quek, P. Renaud, R. J. Black, B. L. Daniel, and M. R. Cutkosky, "An optical actuation system and curvature sensor for a MR-compatible active needle," in *2012 IEEE International Conference on Robotics and Automation*, 2012: IEEE, pp. 1589-1594.

[5] R. Xu, A. Yurkewich, and R. V. Patel, "Curvature, torsion, and force sensing in continuum robots using helically wrapped FBG sensors," *IEEE Robotics and Automation Letters*, vol. 1, no. 2, pp. 1052-1059, 2016.

[6] Y. Hao *et al.*, "A soft gripper with programmable effective length, tactile and curvature sensory feedback," *Smart Materials and Structures*, vol. 29, no. 3, p. 035006, 2020.

[7] S. Ozel, N. A. Keskin, D. Khea, and C. D. Onal, "A precise embedded curvature sensor module for soft-bodied robots," *Sensors and Actuators A: Physical*, vol. 236, pp. 349-356, 2015.

[8] Q. Wang and Y. Liu, "Review of optical fiber bending/curvature sensor," *Measurement*, vol. 130, pp. 161-176, 2018.

[9] I. Floris, J. M. Adam, P. A. Calderón, and S. Sales, "Fiber optic shape sensors: A comprehensive review," *Optics and Lasers in Engineering*, vol. 139, p. 106508, 2021.

[10] L. Mao, P. Lu, Z. Lao, D. Liu, and J. Zhang, "Highly sensitive curvature sensor based on single-mode fiber using core-offset splicing," *Optics & Laser Technology*, vol. 57, pp. 39-43, 2014.

[11] S. Hu, S.-k. Li, and Y. Zhao, "One dimensional vector curvature sensor based on 2-core fiber offset structure," *Measurement*, vol. 193, p. 110964, 2022.

[12] S. Silva *et al.*, "Temperature and strain-independent curvature sensor based on a singlemode/multimode fiber optic structure," *Measurement science and technology*, vol. 22, no. 8, p. 085201, 2011.

[13] Y. Wu *et al.*, "Highly sensitive curvature sensor based on asymmetrical twin core fiber and multimode fiber," *Optics & Laser Technology*, vol. 92, pp. 74-79, 2017.

[14] X. Yang *et al.*, "Highly sensitive curvature sensor based on a sandwich multimode fiber Mach–Zehnder interferometer," *Optics Express*, vol. 30, no. 22, pp. 40251-40264, 2022.

[15] H. Li, H. Li, F. Meng, X. Lou, and L. Zhu, "All-fiber MZI sensor based on seven-core fiber and fiber ball symmetrical structure," *Optics and Lasers in Engineering*, vol. 112, pp. 1-6, 2019.

[16] O. Arrizabalaga *et al.*, "High-performance vector bending and orientation distinguishing curvature sensor based on asymmetric coupled multi-core fibre," *Scientific Reports*, vol. 10, no. 1, pp. 1-10, 2020.

[17] Q. Wang and Y. Liu, "Optical fiber curvature sensor based on MMF-SCF-MMF structure," *Optical fiber technology*, vol. 43, pp. 1-5, 2018.

[18] M. Jang, J. S. Kim, S. H. Um, S. Yang, and J. Kim, "Ultra-high curvature sensors for multi-bend structures using fiber Bragg gratings," *Optics express*, vol. 27, no. 3, pp. 2074-2084, 2019.

[19] J. Ge, A. E. James, L. Xu, Y. Chen, K.-W. Kwok, and M. P. Fok, "Bidirectional soft silicone curvature sensor based on off-centered embedded fiber Bragg grating," *IEEE Photonics Technology Letters*, vol. 28, no. 20, pp. 2237-2240, 2016.

[20] F. Zhu *et al.*, "Stress-insensitive vector curvature sensor based on a single fiber Bragg grating," *Optical Fiber Technology*, vol. 54, p. 102133, 2020.

[21] Y. S. Yu, Z. Y. Zhao, Z. C. Zhuo, W. Zheng, Y. Qian, and Y. S. Zhang, "Bend sensor using an embedded etched fiber Bragg grating," *Microwave and Optical Technology Letters*, vol. 43, no. 5, pp. 414-417, 2004.

[22] H. Wang, R. Zhang, W. Chen, X. Liang, and R. Pfeifer, "Shape detection algorithm for soft manipulator based on fiber bragg gratings," *IEEE/ASME Transactions on Mechatronics*, vol. 21, no. 6, pp. 2977-2982, 2016.

[23] W. Zhou, Y. Zhou, X. Dong, L.-Y. Shao, J. Cheng, and J. Albert, "Fiber-optic curvature sensor based on cladding-mode Bragg grating excited by fiber multimode interferometer," *IEEE Photonics Journal*, vol. 4, no. 3, pp. 1051-1057, 2012.

[24] L.-Y. Shao, A. Laronche, M. Smietana, P. Mikulic, W. J. Bock, and J. Albert, "Highly sensitive bend sensor with hybrid long-period and tilted fiber Bragg grating," *Optics Communications*, vol. 283, no. 13, pp. 2690-2694, 2010.

[25] L. Xu, N. Liu, J. Ge, X. Wang, and M. P. Fok, "Stretchable fiber-Bragg-grating-based sensor," *Optics letters*, vol. 43, no. 11, pp. 2503-2506, 2018.

[26] N. Wu *et al.*, "Microwave photonics interrogation for multiplexing fiber Fabry-Perot sensors," *Optics Express*, vol. 29, no. 11, pp. 16652-16664, 2021.

[27] J. Mora *et al.*, "Photonic microwave tunable single-bandpass filter based on a Mach-Zehnder interferometer," *Journal of lightwave technology*, vol. 24, no. 7, p. 2500, 2006.

[28] X. Zhang *et al.*, "Transition of Fabry–Perot and antiresonant mechanisms via a SMF-capillary-SMF structure," *Optics letters*, vol. 43, no. 10, pp. 2268-2271, 2018.

[29] H. Chen, S. Zhang, H. Fu, B. Zhou, and N. Chen, "Sensing interrogation technique for fiber-optic interferometer type of sensors based on a single-passband RF filter," *Optics Express*, vol. 24, no. 3, pp. 2765-2773, 2016.